


# The use of biotite trace element compositions for fingerprinting magma batches at Las Cañadas volcano, Tenerife

**Journal Article****Author(s):**

[Sliwinski, Jakob](#) ; Ellis, Ben S.; Dávila-Harris, Pablo; Wolff, John A.; Olin, Paul H.; Bachmann, Olivier

**Publication date:**

2017-01

**Permanent link:**

<https://doi.org/https://doi.org/10.3929/ethz-b-000326411>

**Rights / license:**

[In Copyright - Non-Commercial Use Permitted](#)

**Originally published in:**

Bulletin of Volcanology 79(1), <https://doi.org/10.1007/s00445-016-1088-2>

**Funding acknowledgement:**

- Understanding eruptive and post-eruptive processes in rhyolites via lithium (Li) isotopes ()

# The use of biotite trace element compositions for fingerprinting magma batches at Las Cañadas volcano, Tenerife

J. T. Sliwinski<sup>1</sup> · B. S. Ellis<sup>1</sup> · P. Dávila-Harris<sup>2</sup> · J. A. Wolff<sup>3</sup> · P. H. Olin<sup>4</sup> · O. Bachmann<sup>1</sup>

Received: 10 June 2016 / Accepted: 27 November 2016 / Published online: 6 December 2016  
© Springer-Verlag Berlin Heidelberg 2016

**Abstract** Accurate identification of individual volcanic events in the field is crucial for constraining eruption volumes and calculating recurrence intervals between eruptive episodes. Due to complexities of pyroclastic transport and deposition and intra-unit textural variability, such identification can be challenging. We present a novel method for fingerprinting ignimbrites via trace element chemistry (V, Co, Nb) in biotite by laser ablation inductively coupled plasma mass spectrometry (LA-ICP-MS). Using samples from the alkaline magmatic series of Tenerife, we are able to demonstrate (1) clustering of previously characterized units into distinct, homogeneous groups based on V, Co, and Nb concentrations in biotite, despite the presence of extreme variation and zonation in other trace elements (Ba, Sr, Rb) that indicate complex petrogenetic processes, and (2) biotite compositions are similar throughout a deposit and relatively independent of stratigraphic height or juvenile clast texture (crystal-rich vs crystal-poor). Our results show that trace elements in biotite can be used to fingerprint

eruptions and correlate geographically separated volcanic deposits, including those preserved in offshore turbidite records.

**Keywords** Stratigraphy · Tenerife · Alkaline magmatism · Trace element chemistry · Biotite

## Introduction

Constraining the eruptive history of a volcano is a first-order requirement for understanding its behavior and associated hazards, particularly with respect to the magnitude and recurrence rate of eruptive events. Reconstructing eruptive flux (i.e., time/volume relations) relies upon confident correlation of deposits from individual eruptions in both distal and proximal areas and across a variety of depositional environments from the caldera margins to deep-sea settings (Menard 1956; Martí et al. 1994; Schmincke and Sumita 1998). For the largest and most explosive eruptions, the complexity associated with pyroclastic transport and deposition of ignimbrites hampers both correlation on the basis of field appearance and volume estimates based on a real extent (Branney and Kokelaar 2002; Mason et al. 2004). A solution to this comes in the form of geochemical and isotopic studies which can be used to “fingerprint” or identify magma batches and discriminate them from one another. Fingerprinting can be achieved by examining major and trace elements in bulk rock, glass, or minerals (Waters 1961; De Silva and Francis 1989; Smith et al. 2002; Shane et al. 2003; Ukstins-Peate et al. 2003; Harangi et al. 2005; Smith et al. 2011b; Ellis et al. 2012), radiogenic isotopic (Francalanci et al. 1993), or paleomagnetic signatures (Ort et al. 2015). Such studies are increasingly coupled with high-precision geochronology, most typically using <sup>40</sup>Ar/<sup>39</sup>Ar or the U/Pb isotopic systems to distinguish

Editorial responsibility: P. Wallace

**Electronic supplementary material** The online version of this article (doi:10.1007/s00445-016-1088-2) contains supplementary material, which is available to authorized users.

✉ J. T. Sliwinski  
jakub.sliwinski@erdw.ethz.ch

- <sup>1</sup> Institute of Geochemistry and Petrology, ETH Zürich, Clausiusstrasse 25, 8092 Zürich, Switzerland
- <sup>2</sup> Applied Geoscience Department, Instituto Potosino de Investigación Científica y Tecnológica, 78216 San Luis Potosí, Mexico
- <sup>3</sup> School of the Environment, Washington State University, Pullman, WA 99164, USA
- <sup>4</sup> CODES Center of Excellence and School of Physical Sciences, University of Tasmania, Private Bag 79, Hobart, TAS 7001, Australia

the products of individual eruptions (McIntosh et al. 1990; Schoene et al. 2010; Mark et al. 2014; Wotzlav et al. 2014).

While geochemical methods can be powerful, efforts to fingerprint ignimbrites may be complicated as many ignimbrites are known to show compositional zonation as a result of fractional crystallization, pre-eruptive magma mixing (Dorais et al. 1991; Bryan et al. 1998; Eichelberger et al. 2000; Bryan et al. 2002; Olin 2007), or remelting a cumulate pile via the heat and volatile flux from a recharging magma (Bachmann et al. 2014; Forni et al. 2015; Sliwinski et al. 2015; Wolff et al. 2015). While many styles of compositional zonation may occur, a commonly observed form is early erupted, crystal-poor, and more evolved material followed by late-erupted, crystal-rich, and less evolved material (Lipman 1967; Hildreth 1979; Hildreth 1981; Wolff and Storey 1984; Wörner and Schmincke 1984; Mahood and Hildreth 1986; Bachmann et al. 2014; Williams et al. 2014). In such cases, significant differences in bulk major and trace element concentrations are observed between the two types of eruptive products, as are differences in glass chemistry. This complexity in the field and in composition hinders attempts to geochemically link widely separated deposits, which necessitates a fingerprinting method that is robust and unaffected by chemical gradients. Mineral major and trace element compositions are a good candidate and have been the focus of multiple studies.

Biotite chemistry in particular has been recognized as a powerful correlation tool by several authors, all focusing on major element chemistry within chemically unzoned ignimbrites and bentonites. Desborough et al. (1973) used electron probe microanalysis (EPMA) of biotites to correlate volcanic units in the Eocene Green River Formation (USA). Yen and Goodwin (1976) followed up on this work, using X-ray fluorescence (XRF) analyses on bulk biotite separates. Later, in a case study from the Central Andes, de Silva and Francis (1989) demonstrated both the correlation and anticorrelation among a group of homogeneous ignimbrites by biotite major elements in a way that helped to constrain eruptive volume estimates. Haynes et al. (1995) similarly used EPMA to distinguish Ordovician bentonite layers in Sweden and the USA, demonstrating the ability of biotites to retain compositional information even following heavy alteration. More recently, the same method was used by Smith et al. (2011b) and Shane et al. (2003) to correlate volcanic ashes from the Toba eruptions and the Okataina/Taupo volcanic zones, respectively. In the present study, we further investigate biotite, this time utilizing laser ablation inductively coupled plasma mass spectrometry (LA-ICP-MS) analysis of trace elements from a suite of petrographically complex, zoned, and unzoned phonolites on the island of Tenerife (Canary Islands, Spain). We evaluate the signatures recorded by biotite trace element compositions and the extent to which these compositions may be used for correlation purposes.

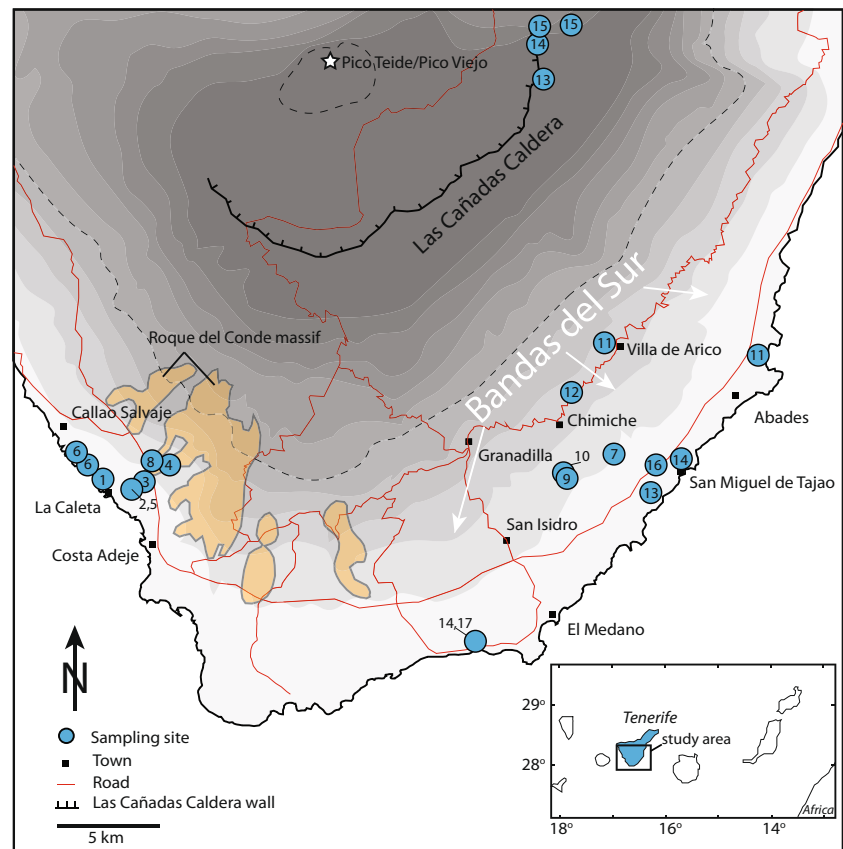
## Geological background

The island of Tenerife is located at the center of the Canary Islands, a hotspot-related ~Miocene–recent ocean island archipelago located 750 km west of the Moroccan coast. The eruptive history of Tenerife began with a succession of basaltic to basanitic shield lavas (at least as old as 11.6 Ma), which, following a period of repose, gave rise to more evolved trachyphonolitic to phonolitic products at ~3 Ma (Ancochea et al. 1990; Ancochea et al. 1999). The western islands, including Tenerife, are constructed upon ~7 km of tholeiitic Jurassic oceanic crust and several kilometers of sediments from the African passive margin. There is no evidence of significant contribution of these reservoirs into Canarian magmas (Robertson and Stillman 1979; Hoernle 1998).

Voluminous phonolitic ignimbrites and fallout deposits erupted from the Las Cañadas caldera (Fig. 1) on Tenerife from 1.8 Ma onwards. They form thick pyroclastic sequences on the southern flanks of the island (Bandas del Sur, Fig. 1) and in the caldera wall. This phase of activity comprises the upper group of the Las Cañadas edifice (Martí et al. 1994) and is further subdivided into three cycles (the Ucanca, Guajara, and Diego Hernández formations, see Edgar et al. (2007)), with each cycle, in turn, consisting of numerous ignimbrites and pumice fall deposits (Walker 1981; Wolff 1985; Blanco 1989; Martí et al. 1990; Mitjavila 1990; Martí et al. 1994; Bryan et al. 1998; Bryan et al. 2002; Brown et al. 2003; Edgar et al. 2007; Dávila-Harris 2009; Dávila-Harris et al. 2013). Caldera-forming volcanism characterized many units in these cycles, leaving overlapping caldera structures at the center of the island, the largest of which led into eruptive hiatuses of hundreds of thousands of years (Martí et al. 1994; Dávila-Harris 2009). Deposition of ignimbrites is clearly topographically controlled, as the southeastern and southwestern deposits form two disconnected sequences separated by the Roque del Conde massif (Fig. 1).

The field appearance of southern Tenerife ignimbrites can be highly variable, both between and within units. Units may differ, for example, on the basis of color, crystal content, lithic horizons, degree of welding, juvenile clast component, and amount of associated fall deposits. Within units, similar variability may occur. For example, the Granadilla Member is remarkably homogeneous in appearance (e.g., low phenocryst abundance, low abundance of lithics and juvenile clasts) and only mildly zoned in chemical composition (Wolff and Storey 1984; Bryan 2006), while the Adeje, Abrigo, Poris, and Enramada units display strong textural and chemical zonation between subunits (Bryan et al. 1998; Edgar et al. 2002; Brown et al. 2003; Dávila-Harris 2009; Dávila-Harris et al. 2013) and often contain juvenile clasts of variable chemical and textural character (Fig. 2). Mixing plays a prominent role in the evolution of Tenerife magmas, as evidenced by the presence of compositional bands in pumices (Edgar et al. 2002), frequent

**Fig. 1** Location of study area and sampling sites in the southern Tenerife. Sampling locations detailed in Table 1. The Bandas del Sur region extends across the southeastern coast of Tenerife and is part of a larger pyroclastic apron that extends westward beyond the topographic spur of the Roques del Conde massif. Roads and major towns shown for reference. Contours represent 200 m. Canary Islands and African coast, with study area highlighted (*inset*)



coexistence of multiple crystal assemblages (mafic and evolved) within single ignimbrites (Wolff 1985) as well as mineral zoning patterns indicating growth under variable chemical conditions (Albert et al. 2015). Degree of welding varies greatly between units, and some (e.g., the Arico Member) additionally feature variably welded zones with a range of coloration (Brown et al. 2003). Although at first glance, the diversity in products seems to aid in distinguishing one unit from another, the intra-ignimbrite diversity may actually serve to complicate potential correlations, particularly if outcrops are widely spaced and record different facies of a given ignimbrite.

Regarding mineralogy and geochemistry, phonolites of southern Tenerife share many similarities despite their variability in field appearance. Bulk major element compositions are comparable across the island with minor variations in SiO<sub>2</sub> (Wolff et al. 2000; Edgar et al. 2002; Brown and Branney 2004a; Bryan 2006; Dávila-Harris et al. 2013), while trace elements (e.g., Ba, Sr) may vary by orders of magnitude (Edgar et al. 2002; Dávila-Harris et al. 2013; Sliwinski et al. 2015). Nb and Zr compositions can be used to identify two distinct phonolite series within the Diego Hernández Formation (Wolff et al. 2000; Edgar et al. 2007). The mineralogy of these phonolites shows minor variability around a consistent assemblage of anorthoclase-sanidine + salite + biotite + magnetite + titanite ± ilmenite ± sodalite-haüyne ±

nepheline (Wolff 1985; Bryan et al. 2002; Edgar et al. 2007). Many units contain crystals derived from mixing with mafic magmas, such as kaersutite, plagioclase, titanite, and olivine (Wolff 1985). Feldspar and pyroxene grains are often zoned in both major and trace elements (Bryan et al. 2002; Sliwinski et al. 2015). While these authors present biotite major element data, biotite trace element variations have been underexplored and are therefore the focus of this work.

## Methods

Juvenile clasts were collected from all three eruptive cycles in southern Tenerife (Fig. 1, Table 1). In particular, the Abrigo, Caleta, Arafo, Poris, and Aldea Members of the Diego Hernández Formation (representing the latest eruptive cycle) were sampled, as well as the Arico and Granadilla Members of the Guajara (middle) cycle. The Monjas, Mocán, Adeje, Barco, San Juan, Agua, Morro, Enramada, Morteros, and Gaviotas ignimbrites (Dávila-Harris 2009) of the Ucanca Formation were also sampled. Biotite phenocrysts were obtained from crushed juvenile clasts which were selected based on the lack of physical alteration or compositional banding. When necessary, dilute methylene iodide ( $\rho = 2.8 \text{ g cm}^{-3}$ ) was used to prepare a heavy mineral separate of the sample. Biotite phenocrysts were then mounted in epoxy and polished with

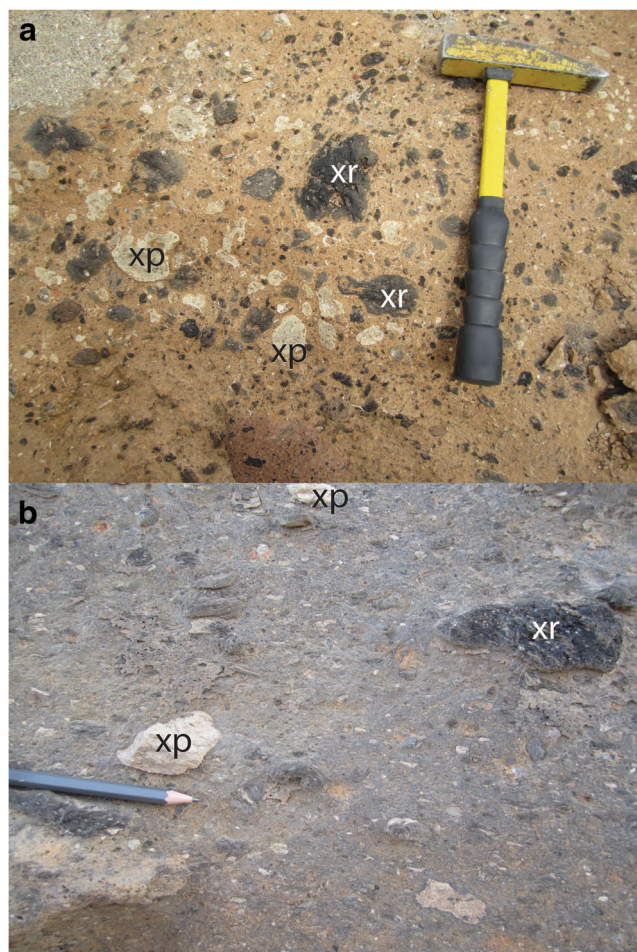


**Fig. 2** Field appearance of the **a** Adeje and **b** Arico ignimbrites. Note variability in juvenile clast components: Crystal-rich (*xr*) clasts (sometimes banded) co-exist with crystal-poor (*xp*) clasts

diamond paste. Imaging of compositional zoning was done by scanning electron microscopy (SEM) in backscatter electron (BSE) mode (Fig. 3).

Major elements in biotite were obtained by electron microprobe (EPMA) at ETH Zürich using a JEOL JXA-8200 at 15 kV acceleration voltage with 15 nA current and 5  $\mu\text{m}$  spot size. Peak and background counting times were 20 s for all elements (F, Na, Mg, Al, K, Ti, Si, Fe, Mn, and Ba). All analyses were corrected with a Phi-Rho-Z scheme and normalized to 22 O. Data quality was monitored using secondary standards from ETH's standard collection, including a natural biotite (H043) and synthetic phlogopite (H088).

Trace elements were obtained by LA-ICP-MS at ETH Zürich using a 193-nm Resonetics ArF excimer laser coupled with a Thermo Element XR ICP-MS. Analysis parameters were 30- $\mu\text{m}$  spot size,  $\sim 3.5 \text{ J cm}^{-2}$ , three cleaning pulses; 5 Hz repetition rate; 20-s background measurement; and 32-s ablation time. Analyses were bracketed and drift corrected with NIST-612 or NIST-610 synthetic glass standard and monitored using the GSD-1G basaltic glass standard. Data were normalized to internal standard element Al or Si

obtained by EPMA (with no appreciable difference between the results of the two standardizations; see [supplement S2](#)) and reduced in the MATLAB-based SILLS program (Guillong et al. 2008). Because of low variability of  $\text{Al}_2\text{O}_3$  and  $\text{SiO}_2$  concentrations, average values per unit were used. When EPMA data were not available, an  $\text{Al}_2\text{O}_3$  value of 13 wt% (representing the overall average of Tenerife biotites) was used. Reproducibility of homogeneous glass standards yields precision better than 5% relative standard deviation (RSD) for elements well above the limit of detection.

## Results

Biotite grains in all units vary between equant and elongated habits, span a size range of 0.1–5.0 mm, and contain inclusions of apatite, oxides, and melt. Complex zoning patterns are visible by BSE and can be subdivided into four categories: (1) simple grains with no BSE brightness variations; (2) grains with two or more distinct and sharply delineated zones with clear differences in BSE brightness (Fig. 3e, f); (3) grains with irregular, zoning textures, consistent with a history involving resorption (Fig. 3a–d); and (4) grains with any combination of the above characteristics. All pumice samples contain both homogeneous biotites and those with complex zonation. It is noteworthy that while the co-occurrence of zoned and unzoned biotites is common, the proportions of the two types may vary markedly from unit to unit.

## Major elements

Major and trace elements in biotite are reported in Table 2. Biotites typically contain 35–39 wt%  $\text{SiO}_2$  and 11–14 wt%  $\text{Al}_2\text{O}_3$  and have Mg number ( $100 \times [\text{mol Mg}] / [\text{mol Mg} + \text{Fe}]$ ) between 55 and 76 (Fig. 4).  $\text{TiO}_2$  among Bandas del Sur biotites varies between  $\sim 5$  and 8 wt% and may show a 1–2 wt% spread within individual units. The stark BSE zonation apparent in some biotites (Fig. 3) is not strongly reflected in major element chemistry. Although some distinctions may be made between units based on major elemental compositions, biotites in many units overlap (Fig. 4).

## Trace elements

Both incompatible (e.g., Rb) and compatible (e.g., Sr, Ba) trace elements vary greatly in biotites from units of the Tenerife system (Figs. 5 and 6). Rb, inversely correlated with Ba and Sr, shows a threefold to fivefold range in most units, while Ba and Sr vary over nearly two orders of magnitude. It is worth noting here that in Ba–Sr space, the population of all Tenerife biotites forms two trends: a high Ba trend (slope  $\sim 2700$ ) and a low Ba trend (slope  $\sim 500$ ). Such trends were known from bulk-rock data (Ablay et al. 1998; Olin 2007) and

**Table 1** Unit coordinates and ages

Unit	Cycle <sup>a</sup>	Age $\pm \sigma$ (Ma)	Easting <sup>b</sup>	Northing <sup>b</sup>	Ref.	Location
El Abrigo	DHF III	0.169 $\pm$ 0.001	345,398	3,101,985	Brown et al. (2003)	17
La Caleta	DHF II	0.221 $\pm$ 0.005	354,765	3,109,920	Brown et al. (2003)	16
Arafo	DHF II		347,889	3,129,886		15
			349,751	3,130,197		
Poris	DHF I	0.271 $\pm$ 0.006 <sup>c</sup>	355,506	3,110,406	Brown et al. (2003)	14
			348,027	3,129,242		
			345,600	3,101,800		
Aldea	DHF I	0.334 $\pm$ 0.005	354,789	3,109,421	Edgar et al. (2007)	13
			348,206	3,127,793		
Granadilla	Guajara	0.600 $\pm$ 0.007	349,748	3,113,411	Brown et al. (2003)	12
Arico	Guajara	0.668 $\pm$ 0.008	359,220	3,116,004	Brown et al. (2003)	11
			352,218	3,116,736		
Monjas	Ucanca	1.310 $\pm$ 0.006	349,675	3,110,449	Dávila-Harris (2009)	10
Mocan	Ucanca	1.494 $\pm$ 0.008	350,152	3,109,934	Dávila-Harris (2009)	9
Adeje	Ucanca	1.559 $\pm$ 0.014	329,381	3,110,568	Dávila-Harris et al. (2013)	8
Barco	Ucanca	1.601 $\pm$ 0.008	352,526	3,111,143	Dávila-Harris (2009)	7
San Juan	Ucanca	1.50 $\pm$ 0.03	326,269	3,110,808	Huertas et al. (2002)	6
			325,634	3,111,563		
Agua	Ucanca	Unknown	330,410	3,110,856		5
Morro	Ucanca	Unknown	330,410	3,110,856		4
Enramada	Ucanca	1.661 $\pm$ 0.02	328,508	3,109,600	Dávila-Harris (2009)	3
Morteros	Ucanca	Unknown	328,508	3,109,600		2
Gaviotas	Ucanca	1.84 $\pm$ 0.07	326,988	3,110,134	Huertas et al. (2002)	1

*DHF* Diego Hernandez Formation

<sup>a</sup> Eruptive cycles according to Edgar et al. (2007)

<sup>b</sup> UTM zone 28R, datum WGS84

<sup>c</sup> Member 9 of Brown et al. (2003) and “Upper Gray Member” of Bryan et al. (1998)

were also observed in feldspars among a subset of the units sampled here (Sliwinski et al. 2015).

While concentrations of some trace elements vary enormously, others exhibit relatively low variability in these biotites, particularly V, Co, and Nb (Table 2, S1). However, their concentrations can differ significantly between different ignimbrites (Figs. 6 and 7, Table 2), allowing fingerprinting. V, Co, and Nb concentrations are largely unaffected by complex zoning in biotites, while Ba and Sr concentrations may vary by orders of magnitude along a well-defined trend (Fig. 6). Repeated analysis of multiple samples within units (with variable crystal contents) suggests that V–Co–Nb concentrations are unaffected by crystallinity (see Poris and Arico units) or by spatial separation of outcrops (e.g., large lateral distance between sampling outcrops within Poris, Caleta, Arafo, Aldea, and Arico Members). Only biotites from the Monjas and Mocán units, which notably contain low modal proportions of biotite (necessitating heavy liquid separation), display extremely heterogeneous trace element compositions, potentially due to entrainment of xenocrysts. Biotites from the La Caleta and Arafo units (both in the Diego Hernandez

Formation II of Edgar et al. (2007)) plot in overlapping fields, which are distinct from those of other Diego Hernández units (e.g., El Abrigo, Poris, Aldea). Ten samples from the Poris unit (representing a wide range in crystallinities and many sampling locations) display more variability in V than other southern Tenerife units but are still relatively restricted and discernible in the Co and Nb dimensions (Figs. 6 and 7). However, some overlap does occur between the Abrigo and Poris units, suggesting that multiple lines of evidence are occasionally necessary (e.g., geochronology, glass data, whole rock data) in order to make a positive identification.

## Discussion

These complex biotites from Tenerife record a rich magmatic history, involving disequilibrium textures, extreme compositional variability in some trace elements, and remarkable homogeneity in others. The paths to such characteristics are discussed below.

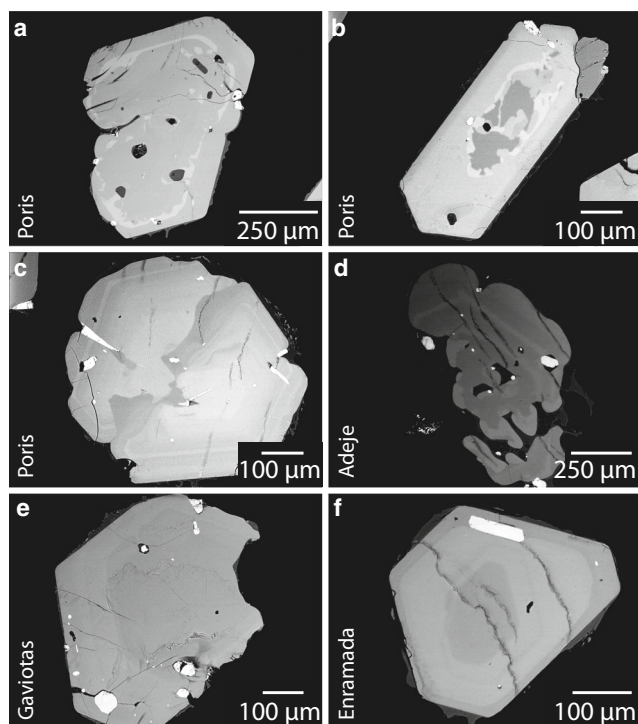


**Fig. 3** Backscatter electron images of biotite phenocrysts, showing variable degrees of resorption and zonation: **a–c** Poris biotite, **d** Adeje biotite, **e** Gaviotas biotite, and **f** Enramada biotite

### Biotites as recorders of petrogenetic processes

It has recently been suggested that the crystal-rich juvenile clasts observed in many Tenerife ignimbrites (e.g., Arico, Adeje; Fig. 2) are produced via remobilization of a crystal-rich “mushy” portion at the base of the magma reservoir following recharge by hotter magma. Evidence for this process has been presented in the form of whole rock compositions (Wolff et al. 2015) and from mineral chemistry, particularly in feldspar (Sliwinski et al. 2015). The striking zoning patterns of biotites with embayed BSE darker core and the BSE brighter rim are consistent with such an origin involving remobilization from an evolved cumulate pile that was reheated and partially remelted. The extreme variability in the compatible elements (e.g., Ba increasing by a factor of up to 50 from the core to the rim of a single biotite) not only suggests locally enriched melts following this melting event (Sliwinski et al. 2015; Wolff et al. 2015) but also agrees with abundant evidence for mixing of different magma batches made on Tenerife (Wolff 1985; Araña et al. 1994; Ablay et al. 1998; Bryan et al. 2002; Edgar et al. 2002; Olin 2007).

In this dynamic and open system, the restricted variability of Nb, V, and Co among and within biotites preserved in samples with large variations in chemical compositions and crystallinities is a remarkable feature. In particular, bimodal units (e.g., the Arico, Poris) which contain dark, crystal-rich clasts and light, crystal-poor clasts vary dramatically in whole

rock trace element composition (Fig. 8; see also Dávila-Harris 2009; Sliwinski et al. 2015) but only nominally in biotite trace element (Nb, Co, V) composition (Figs. 7 and 8c). It implies that such elements are not partitioned strongly between melt and crystals (bulk  $D \sim 1$ ) while biotite is crystallizing. To counterbalance the abundance of alkali feldspars, which have very low partition coefficients for these elements, some quantity of minerals such as Fe–Ti oxides, clinopyroxene, amphibole, and titanite, in which those elements partition more strongly, is needed. These minerals are typically not modally abundant, but as the partition coefficients can be high, a few modal percent of those phases are sufficient to keep bulk  $D \sim 1$ . Trace transition metals, for example, partition into pyroxene and biotite with  $D$ s in the range of  $\sim 1$ –10 (Ewart and Griffin 1994) but only account for  $\sim 5\%$  of the crystallizing assemblage, meaning that they contribute a *maximum* of  $\sim 0.5$  to the bulk  $D$ . Titanite has a partition coefficient of 32–43 for Nb (Olin and Wolff 2012), while spinel has partition coefficients in the range of 10–50 for trace metals (Luhr and Carmichael 1980; Villemant 1988). However, these phases only comprise a 1–2% of the mineral assemblage and so contribute a *maximum* of  $\sim 1$  to bulk  $D$  for these elements. Furthermore, experimental work on the Abrigo Member suggests that the onset of oxide and titanite crystallization precede and follow biotite crystallization, respectively (Andújar et al. 2008), indicating that their competition with biotite for the same trace elements is limited. Finally, while feldspar crystallization drives up incompatible element concentrations (e.g., Nb), the bulk of this modally dominant phase crystallizes after biotite, and Nb signatures remain relatively stable in biotite.

As mentioned previously, there is ample evidence for recharge/mingling preserved in lavas and ignimbrites on Tenerife, and we can infer from the frequency of Holocene and historic basaltic eruptions (Carracedo et al. 2007; Solana 2012) that Tenerife magma reservoir(s) would have been exposed to more primitive input at some or all stages of evolution. As mafic magmas tend to have higher V content than the phonolites ( $\sim 250$ – $400$  ppm, compared to  $<100$  for the phonolites; Thirlwall et al. 2000; Sliwinski et al. 2015), such mafic recharge would be easily recorded in biotite. The fact that they typically show limited variation suggests that *mafic* recharge is limited in terms of mass (although very visible when it occurs as it leaves clear petrographic marks in the form of mingling or multiple phenocryst assemblages). The fact that mafic recharge is volumetrically not dominant does not mean that mixing is uncommon; the addition of intermediate magmas (phonotephrites) from the lower crustal MASH zone commonly happens (i.e., zones of melting, assimilation, storage, and homogenization; see Hildreth and Moorbath 1988), and it forms the bulk of the subvolcanic reservoir, where the phonolites differentiate (Sliwinski et al. 2015).

**Table 2** Biotite major and trace element compositions

Sample	15TF10		15TF16		15TF19		15TF21		15TF23		15TF26	
Unit	Morro		San Juan		Agua		Morteros		Monjas		Mocan	
Major elements (wt%, 2 $\sigma$ )												
SiO <sub>2</sub>	37.91	0.53	36.99	0.77	35.85	0.74	36.97	0.50	36.70	1.77	36.60	1.42
Al <sub>2</sub> O <sub>3</sub>	12.55	0.45	11.88	0.73	12.78	0.59	13.69	0.25	12.06	1.50	11.90	1.05
MgO	15.19	0.54	17.39	0.42	15.44	0.37	14.43	0.62	16.63	2.12	16.58	1.51
FeO	14.19	0.51	10.95	0.66	13.25	0.54	14.55	1.61	12.02	2.17	12.17	2.14
TiO <sub>2</sub>	5.53	0.51	6.15	0.67	6.18	0.50	6.13	0.80	6.07	1.01	5.54	1.45
MnO	0.79	0.07	0.36	0.09	0.55	0.14	0.38	0.14	0.45	0.25	0.58	0.31
Na <sub>2</sub> O	0.91	0.04	1.36	0.10	1.22	0.17	0.90	0.14	1.27	0.24	1.17	0.31
K <sub>2</sub> O	8.96	0.19	8.14	0.26	8.18	0.41	8.95	0.20	8.40	0.23	8.53	0.51
BaO	0.08	0.18	0.86	0.42	0.91	0.74	0.08	0.13	0.55	0.64	0.46	0.70
F	0.51	0.08	1.26	0.20	0.46	0.27	0.28	0.09	1.13	0.67	1.17	0.52
Sum	96.10	1.09	94.09	0.77	94.35	0.91	96.07	1.26	94.15	0.89	93.53	0.50
Mg number	65.61	1.48	73.90	1.27	67.51	1.27	63.88	3.50	71.10	6.20	70.82	5.35
<i>n</i>	9		10		11		8		11		8	
Trace elements (ppm, 2 $\sigma$ )												
P	26	15	27	18	37	21	35	20	40	18	46	32
Ca	575	222	673	502	555	373	773	370	544	90	599	375
Sc	4.0	0.7	5.1	1.7	3.6	1.3	4.5	1.2	4.2	1.8	4.3	1.7
V	93	8	70	38	59	26	205	33	84	66	75	80
Co	7.8	0.6	2.0	8.9	1.8	4.7	40.8	3.8	5.7	15.8	1.7	4.3
Zn	572	190	311	117	431	133	361	97	408	210	841	1878
Ga	28	5	27	5	25	3	27	5	26	5	30	6
Rb	298	147	191	297	220	53	495	166	205	131	300	199
Sr	1.2	1.8	2.4	6.5	3.2	4.3	2.8	3.8	10.5	38.8	2.6	6.4
Y	0.1	0.2	0.2	0.4	0.5	1.6	0.1	0.2	0.3	0.7	0.3	0.4
Zr	15	4	8	14	27	67	37	9	14	19	16	56
Nb	134	13	64	71	120	28	156	13	98	73	101	164
Cs	2.6	6.8	2.4	15.9	1.7	3.6	2.7	3.9	0.8	1.4	2.5	5.1
Ba	638	2302	6460	6000	6915	7401	546	1559	5931	7896	3486	4576
La	0.1	0.5	0.3	1.2	0.7	2.9	0.1	0.2	0.3	0.8	0.5	1.1
Ce	0.5	2.6	0.4	1.6	6.3	31.3	0.7	2.2	2.5	12.0	2.6	4.4
Pb	0.3	0.4	0.2	0.3	1.0	3.7	0.6	0.1	0.4	0.6	1.3	6.2
<i>n</i>	24		28		22		24		22		22	
Sample	15TF27				15TF49				15TF52		15TF34	
Unit	Mocan				Barco				Pegueros		Arico	
Major elements (wt%, 2 $\sigma$ )												
SiO <sub>2</sub>	35.86		1.25		38.26		0.59		36.75		0.77	
Al <sub>2</sub> O <sub>3</sub>	12.73		0.88		12.45		0.53		12.43		0.51	
MgO	14.81		2.76		16.85		0.40		17.16		0.55	
FeO	14.40		3.62		11.51		0.80		10.56		0.48	
TiO <sub>2</sub>	5.61		1.44		6.23		0.65		6.81		0.78	
MnO	0.59		0.25		0.42		0.13		0.32		0.07	
Na <sub>2</sub> O	0.93		0.25		1.23		0.16		1.41		0.13	
K <sub>2</sub> O	8.85		0.37		8.44		0.38		8.19		0.41	
BaO	0.11		0.23		0.47		0.54		0.61		0.65	
F	0.65		0.42		0.96		0.09		1.01		0.21	
Sum	93.90		0.93		95.85		0.78		94.24		1.02	
Mg number	64.63		9.88		72.30		1.62		74.33		1.08	

**Table 2** (continued)

<i>n</i>	21		9		11		10							
Trace elements (ppm, 2σ)														
P	35	18	39	42	40	41	31	25						
Ca	604	169	602	298	517	148	593	257						
Sc	3.0	1.5	5.8	1.1	4.3	0.6	2.3	0.5						
V	181	87	101	29	81	6	140	14						
Co	13.9	17.2	1.3	0.3	3.3	0.3	5.3	0.3						
Zn	480	152	341	113	281	71	535	131						
Ga	28	8	25	5	25	3	29	5						
Rb	403	343	176	103	171	47	373	112						
Sr	2.1	3.9	0.9	1.4	10.5	9.6	0.4	1.0						
Y	0.1	0.2	0.2	0.4	0.1	0.3	0.5	3.3						
Zr	22	21	10	5	11	4	12	8						
Nb	148	62	73	8	82	4	120	6						
Cs	2.6	11.2	0.5	0.7	0.4	0.2	1.4	0.6						
Ba	898	2098	5850	8071	4827	4511	198	444						
La	0.2	0.9	0.3	1.2	0.1	0.4	0.5	3.1						
Ce	0.3	1.0	0.7	2.7	0.2	0.9	0.7	3.0						
Pb	0.4	0.2	0.2	0.2	0.2	0.2	0.2	0.2						
<i>n</i>	25		31		18		30							
Sample Unit	12_030 Arico	12_031 Arico	12_001 Enramada	12_010 Adeje	12_019 Gaviotas	12_043 Poris	12_045 Poris							
Major elements (wt%, 2σ)														
SiO <sub>2</sub>	36.65	0.68	36.96	1.54	37.98	0.90	38.13	0.87	37.68	0.49	36.70	0.80	34.98	1.17
Al <sub>2</sub> O <sub>3</sub>	13.33	0.28	13.22	0.56	12.82	0.33	12.60	0.55	13.07	0.29	13.61	0.36	13.57	0.65
MgO	15.67	0.48	15.92	1.01	16.20	0.59	16.92	0.61	15.32	0.47	14.20	0.57	14.39	0.51
FeO	11.33	0.69	11.33	0.97	10.95	0.45	10.51	0.41	12.99	0.48	14.36	1.09	14.23	1.46
TiO <sub>2</sub>	7.46	0.65	7.28	1.22	7.40	0.54	6.94	0.86	6.34	0.66	6.38	1.16	6.29	1.56
MnO	0.38	0.07	0.39	0.11	0.34	0.06	0.34	0.11	0.52	0.07	0.49	0.14	0.45	0.22
Na <sub>2</sub> O	1.23	0.11	1.23	0.18	1.14	0.10	1.33	0.16	0.95	0.09	0.81	0.10	0.89	0.12
K <sub>2</sub> O	7.84	0.37	8.02	0.88	8.62	0.53	8.37	0.36	8.98	0.19	9.03	0.43	8.73	0.55
BaO	–	–	–	–	–	–	–	–	–	–	–	–	–	–
F	–	–	–	–	–	–	–	–	–	–	–	–	–	–
Sum	93.89	1.12	94.35	2.33	95.45	2.54	95.15	0.99	95.84	0.80	95.58	1.06	94.15	1.04
Mg number	71.14	1.49	71.46	2.44	72.52	0.84	74.15	1.01	67.77	1.11	63.81	2.24	64.32	2.86
<i>n</i>	9		34		31		14		25		31		9	
Trace elements (ppm, 2σ)														
P	80	41	97	88	86	40	81	30	83	39	92	48	34	13
Ca	705	335	537	82	619	311	–	–	551	245	635	224	659	195
Sc	–	–	–	–	–	–	–	–	–	–	–	–	2.9	0.8
V	170	13	168	20	121	6	81	8	106	8	258	38	252	52
Co	4.9	0.7	4.9	0.6	12.2	0.9	3.3	0.5	21.8	1.2	14.2	4.6	19.5	9.5
Zn	305	49	320	107	256	29	272	43	422	22	431	91	429	170
Ga	–	–	–	–	–	–	–	–	–	–	–	–	26	7
Rb	166	44	187	111	131	43	167	38	383	75	227	52	291	190
Sr	4.5	3.9	4.2	6.1	0.7	0.6	12.2	9.5	8.3	4.4	10.2	19.9	15.6	33.2
Y	0.4	1.0	0.3	0.3	0.2	0.5	0.3	0.6	0.2	0.2	0.2	0.3	0.1	0.1
Zr	–	–	–	–	–	–	–	–	–	–	–	–	26	9
Nb	105	8	107	12	75	5	79	6	193	13	162	12	156	30
Cs	0.4	0.2	0.5	0.5	1.4	6.5	0.5	0.9	1.3	0.5	0.7	0.3	1.0	1.0
Ba	14,751	11,757	12,368	15,804	2157	3785	5239	4347	1039	1575	4994	10,488	4766	11,026
La	0.4	1.6	0.2	0.8	0.2	0.9	0.2	0.7	0.2	0.8	0.2	0.9	0.1	0.2
Ce	0.5	3.0	0.4	1.9	0.6	2.4	0.5	1.5	4.6	36.9	0.6	2.5	0.3	0.8
Pb	0.4	0.4	0.4	0.9	0.3	0.1	0.3	0.1	0.6	1.1	0.6	0.6	0.5	0.2
<i>n</i>	33		50		31		15		23		48		22	

### Biotites as correlation tools

The limited variation of V, Nb, and Co in biotites in this study provides a useful means of distinguishing magma batches, particularly in cases where EPMA provides ambiguous

correlation data. In this case, the improved ability to distinguish biotites from different units provides the potential to correlate pyroclastic units across the island from the Bandas del Sur to the north side of Tenerife, where increased rainfall and more rapid weathering negatively affects exposure

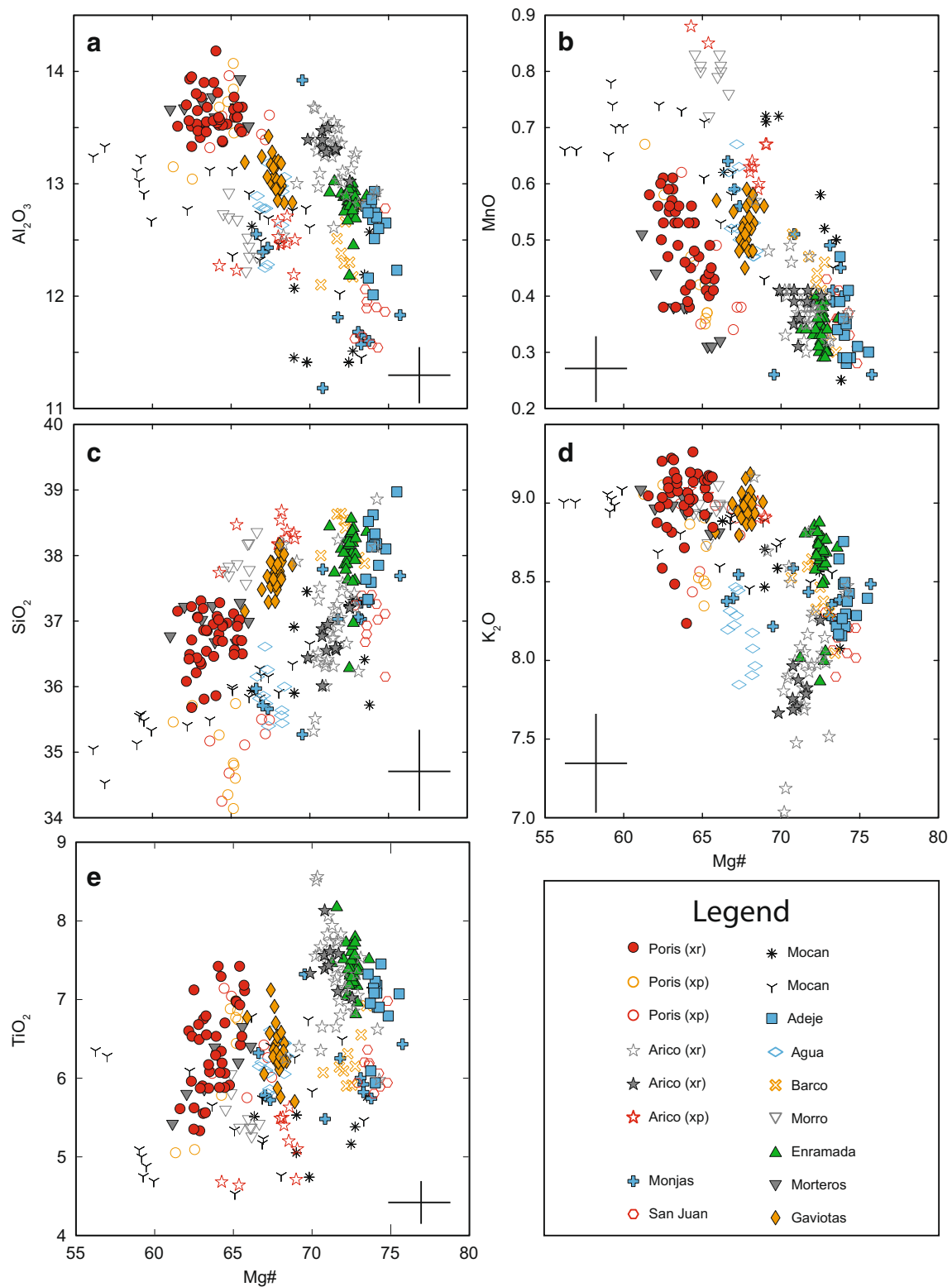


**Fig. 4** Major element compositions of biotites from different Tenerife units, expressed in wt. % oxide. Note that in many cases, major element compositions overlap and separation of units is not possible. Each *symbol*

represents biotites from one juvenile clast sample. *Error bars* represent Huertas  $\pm 2\sigma$  error based on reproducibility of secondary standards

quality. More generally, this approach can be used to correlate distal ashes back to their sources, up to thousands of

kilometers away (Smith et al. 2011b). Furthermore, biotite compositions may aid in linking offshore and subaerial

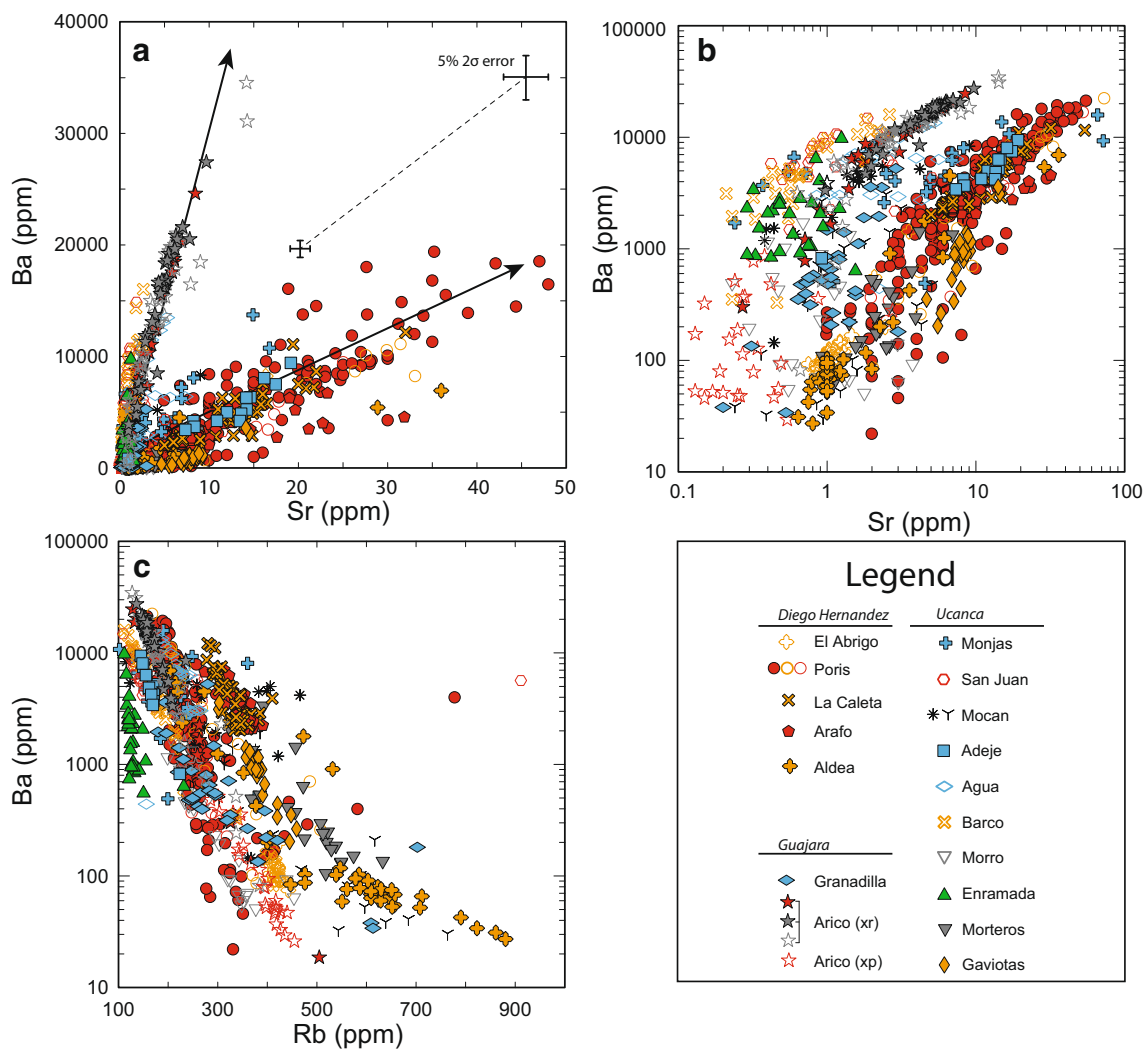


**Fig. 5** Trace element concentration (ppm) of Tenerife biotites: **a**, **b** Sr vs Ba and **c** Rb vs Ba. Error bars in **a** represent maximum  $\pm 2\sigma$  error ( $\sim 5\%$  based on long-term reproducibility of secondary standards). Error bars in logarithmic plots are smaller than symbols

deposits, as well as correlating volcanoclastic turbidites (particularly those that are associated with the degradation of volcanic edifices and are interlayered with volcanic ash). With volcanic islands such as the Canaries being commonly affected by large landslides (Watts and Masson 1995; Schmincke and Sumita 1998; Hunt et al. 2014; Le Friant et al. 2015), the utility of such indicators is clear. Finally, in order to determine accurate eruption volumes, it is necessary to piece together offshore pyroclastic deposits, given that much of the volume in a pyroclastic density current may bypass deposition on land and end up in the sea (Brown and Branney 2004b). The analysis of trace elements in biotite provides additional, often more discriminating, information for these purposes and also sheds light on magmatic processes as discussed above.

Geochemical correlations are typically done by major element chemistry in glass or minerals or by trace element chemistry in glass. While powerful, these techniques have a few drawbacks that may be complemented by an additional

method. Major element chemical variations in minerals are limited by stoichiometry, which allows easier quality control of data and limits the extent of element mobility during analysis. Since major element analysis is anyways necessary for the internal calibration of LA-ICP-MS measurements (i.e., counts registered by the mass spectrometer must be anchored to a major element concentration), this means that obtaining both major element *and* trace element data on minerals is usually more straightforward than for glass. However, the relatively low degree of major element variability in minerals compromises the discriminating potential of the elements (Fig. 4). Trace elements, alternatively, offer large variations between samples, and a broad array of discriminating elements is available for study by LA-ICP-MS. Many authors have successfully demonstrated the use of trace elements in glass to fingerprint ignimbrites (e.g., Sarna-Wojcicki et al. 1984; Westgate et al. 1994; Pearce et al. 1996; Shane 2000; Harangi et al. 2005; Smith et al. 2011a; Szymanowski et al.

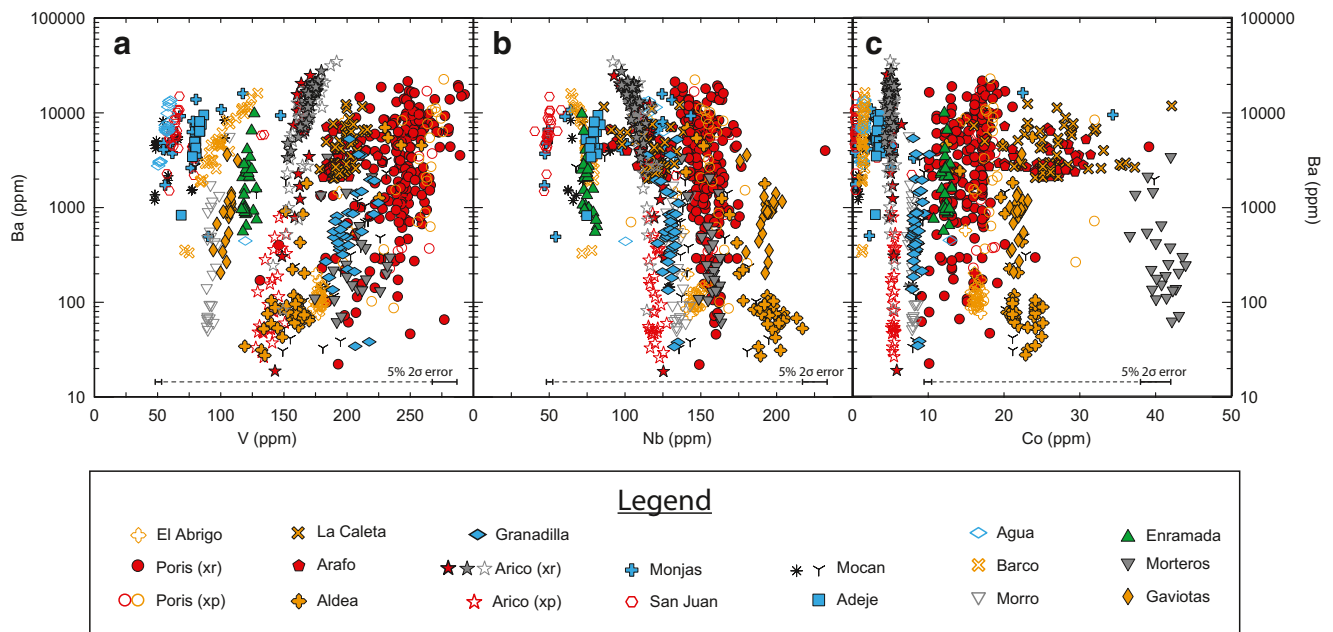


**Fig. 6** Trace element concentrations (ppm) of Tenerife biotites: **a** Ba vs V, **b** Ba vs Nb, and **c** Ba vs Co. Note that despite strong zonation in Ba, the concentrations of V, Co and Nb vary only slightly. Error bars in logarithmic plots are smaller than symbols represent  $5\% \pm 2\sigma$  error across the range of concentrations. Error bars in logarithmic plots are smaller than symbols

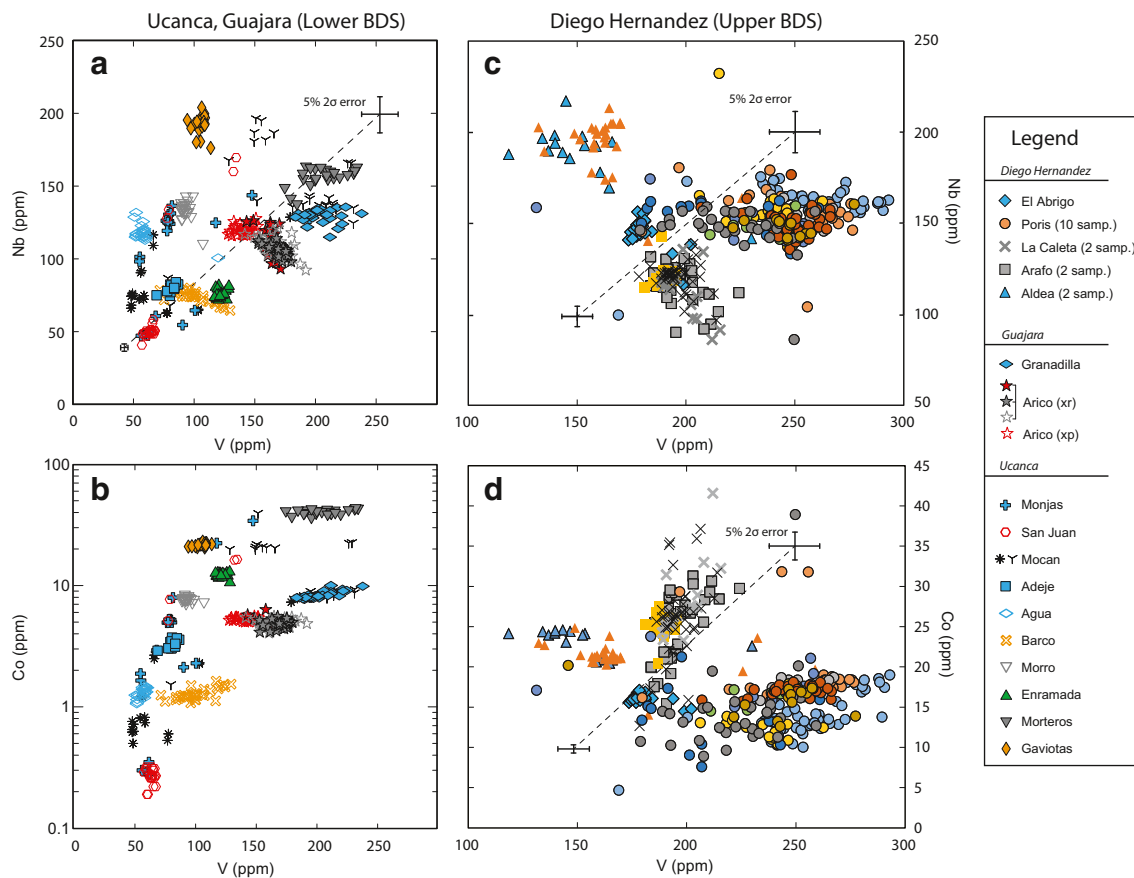


**Fig. 7** Trace element concentrations (ppm) of Bandas del Sur biotites: **a** V vs Nb and **b** V vs Co from the lower two eruptive cycles (Ucanca, Guajara). **c**, **d** V vs Nb and V vs Co for the Diego Hernández Formation of the upper Bandas del Sur. Different symbols indicate different units; colors of symbols represent multiple samples from the same unit. Error bars in **a** represent range of  $5\% 2\sigma$  errors from low to high concentrations. Error bars in logarithmic plots are smaller than symbols

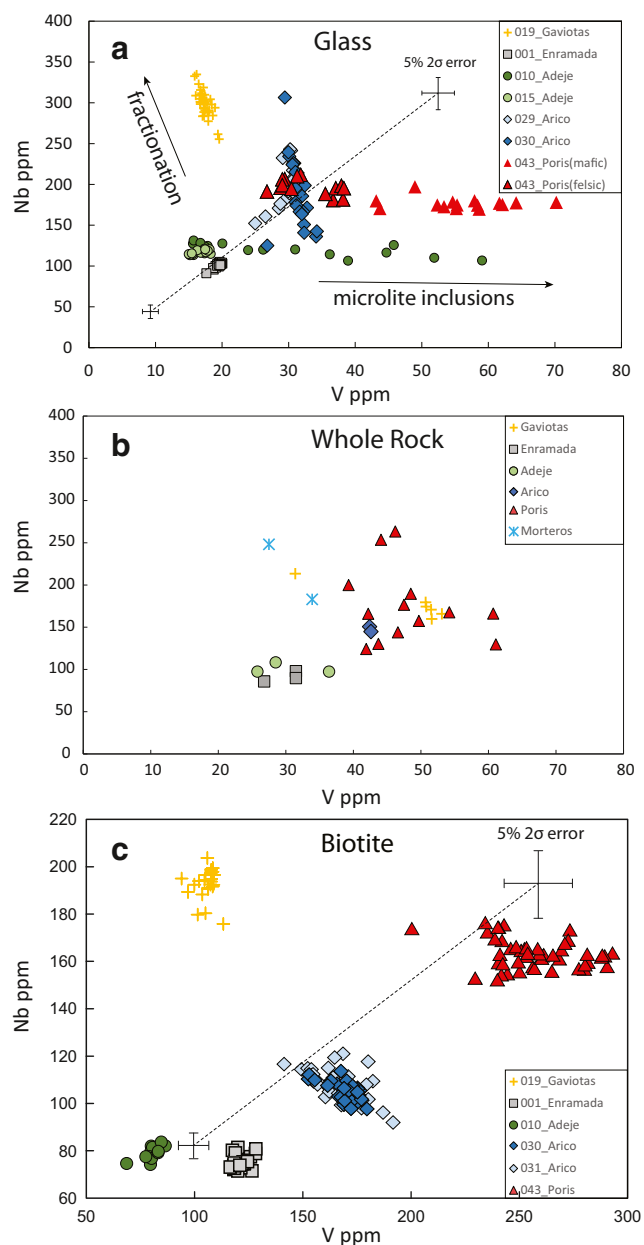


**Fig. 8** Trace element discrimination diagrams using **a** glass, **b** whole rock and **c** biotite compositions (modified after Sliwinski 2014). Note (1) clear separation between units using biotite compositions, (2) poor discrimination using whole rock compositions, and (3) reasonable discrimination using glass compositions. Glass is easily contaminated by microcrysts, here most likely oxide microcrysts which generate a spread in V concentrations. Thick sections (100  $\mu\text{m}$ ) are typically dark, and a priori identification of microcrysts is not possible. Additionally, fractionation trends in glass may lead to increasing Nb concentrations that reduce the discriminating potential of the method

2015; Vidal et al. 2015; Donato et al. 2016), but we note that there are some circumstances in which trace elements in glass or whole rock do not accurately resolve different events (Fig. 8). For the successful analysis of glass, one must be able to find relatively clean and unaltered glass shards, which may be difficult in dark, devitrified, microcrystalline, or weathered

samples. Even if an ignimbrite is unaltered and unwelded, analysis of clean glass compositions may be hindered by the presence of microcrysts that are often more abundant and more difficult to identify during data reduction than mineral/melt inclusions in minerals. Furthermore, the composition of glass may differ dramatically within the same unit (Forni et al. 2016). In this study, V and Co signals in glass are particularly susceptible to contamination by oxide microlites, while Nb signals may be influenced by fractional crystallization (Fig. 8a). Attempting to correlate by whole rock compositions is additionally complicated by variations in crystal content and subsequent large variations in trace element concentrations (Fig. 8b). In such cases, application of biotite trace element chemistry may help to resolve ambiguities in glass data and complement more traditional methods of stratigraphic correlation (Fig. 8c).

### Limitations

Due to the fact that Nb, Co, and V have different valence states and ionic radii and partition strongly into some minerals, the consistency of their signature is remarkable. The use of these elements as discriminators in biotite must be considered on a case-by-case basis, for the following reasons:

1. Co-crystallization of large amounts of a phase that strongly partitions a given element, will preclude that element's utility as a discriminator in biotite.
2. Compositional effects may influence the partition coefficients of these elements in biotite (Hazen and Wones 1972; Dymek 1983). This effect was also documented by Stepanov and Hermann (2013), who in compiling partition coefficients for Nb into biotite from various sources (Nash and Crecraft 1985; Acosta-Vigil et al. 2010) noted a direct relationship between  $\text{TiO}_2$  (1.18–5.59 wt%) and  $D_{\text{Nb}}$  (0.15–9.21). If the partition coefficient of an element into biotite drops too much below 1, the concentrations will decrease and the precision at which we can distinguish groups of biotite from different sources will be significantly affected.
3. Even if the above criteria are satisfied, a given trace element signature may still be unresolvable between units, due to similar parent and petrogenetic histories. A combination of different discriminators is therefore favored.
4. Given that the co-crystallizing mineral assemblage affects the trace element budget and that the major element chemistry of biotite affects its trace element preferences, other discriminators (each with appreciable concentrations in biotite) may prove helpful in other systems. For example, calc-alkaline suites have not been explored in this study and warrant a closer look with other trace element discriminators (e.g., Sc, Cr, Mn, Ni, Cu, Zn, Zr, Hf, and Ta could be analyzed along with V, Nb, and Co).

## Conclusions

Here, we present an improvement in geochemical fingerprinting for correlation purposes in volcanology by analyzing trace metals and high field strength elements in biotite grains by LA-ICP-MS. We find that biotite crystals in the deposits from individual eruptions preserve distinct trace element signatures. In detail,

1. Bandas del Sur/southern Tenerife biotites are remarkably complex and zoned, especially in Ba, Rb, and Sr. Such zoning indicates periods of recharge/mixing, and potentially the remelting of a cumulate pile, but has little effect on trace transition metal concentrations.
2. Trace transition metals (e.g., V, Co, Nb) are homogeneous within biotites from individual eruptions and act as fingerprints of magma batches on Tenerife. This homogeneity is observed both across multiple sampling locations and independently of the petrologic complexity of an ignimbrite. Such homogeneity suggests that the bulk  $D$  for these elements is  $\sim 1$ , at least during the crystallization of biotite.
3. When coupled with major element chemistry, glass compositions, and geochronology, biotite trace element analysis represents a powerful geochemical tool for correlating magma batches (deposits) around the slopes of the volcano and into the offshore turbidite record.

**Acknowledgments** We would like to thank Alina Fiedrich for assistance in the field and Lukas Martin for his help in microprobe analysis. Wolff and Olin's Tenerife work was funded by NSF grant EAR0001013. Sliwinski, Ellis, and Bachmann were funded by Swiss NSF grant 200021\_166281.

## References

- Ablay G, Carroll M, Palmer M, Martí J, Sparks R (1998) Basanite–phonolite lineages of the Teide–Pico Viejo volcanic complex, Tenerife, Canary Islands. *J Petrol* 39:905–936
- Acosta-Vigil A, Buick I, Hermann J, Cesare B, Rubatto D, London D, Morgan GB (2010) Mechanisms of crustal anatexis: a geochemical study of partially melted metapelitic enclaves and host dacite, SE Spain. *J Petrol* 51:785–821
- Albert H, Costa F, Martí J (2015) Timing of magmatic processes and unrest associated with mafic historical monogenetic eruptions in Tenerife Island. *J Petrol* egv058
- Ancochea E, Fuster J, Ibarrola E, Cendrero A, Coello J, Hernan F, Cantagrel J, Jamond C (1990) Volcanic evolution of the island of Tenerife (Canary Islands) in the light of new K–Ar data. *J Volcanol Geotherm Res* 44:231–249
- Ancochea E, Huertas M, Cantagrel J, Coello J, Fúster J, Arnaud N, Ibarrola E (1999) Evolution of the Cañadas edifice and its implications for the origin of the Cañadas caldera (Tenerife, Canary Islands). *J Volcanol Geotherm Res* 88:177–199
- Andújar J, Costa F, Martí J, Wolff JA, Carroll M (2008) Experimental constraints on pre-eruptive conditions of phonolitic magma from the caldera-forming el Abrigo eruption, Tenerife (Canary Islands). *Chem Geol* 257:173–191
- Araña V, Martí J, Aparicio A, García-Cacho L, García-García R (1994) Magma mixing in alkaline magmas: an example from Tenerife, Canary Islands. *Lithos* 32:1–19
- Bachmann O, Deering CD, Lipman PW, Plummer C (2014) Building zoned ignimbrites by recycling silicic cumulates: insight from the 1,000 km<sup>3</sup> Carpenter Ridge Tuff, CO. *Contrib Mineral Petrol* 167:1–13
- Blanco JJA (1989) Estudio volcanoestratigráfico y volcanológico de los piroclastos sálicos de sur de Tenerife: Universidad de La Laguna
- Branney MJ, Kokelaar BP (2002) Pyroclastic density currents and the sedimentation of ignimbrites. Geological Society of London
- Brown RJ, Barry T, Branney M, Pringle M, Bryan S (2003) The quaternary pyroclastic succession of southeast Tenerife, Canary Islands: explosive eruptions, related caldera subsidence, and sector collapse. *Geol Mag* 140:265–288
- Brown RJ, Branney M (2004a) Event-stratigraphy of a caldera-forming ignimbrite eruption on Tenerife: the 273 ka Poris Formation. *Bull Volcanol* 66:392–416
- Brown RJ, Branney MJ (2004b) Bypassing and diachronous deposition from density currents: evidence from a giant regressive bed form in the Poris ignimbrite, Tenerife, Canary Islands. *Geology* 32:445–448
- Bryan S (2006) Petrology and geochemistry of the quaternary caldera-forming, phonolitic Granadilla eruption, Tenerife (Canary Islands). *J Petrol* 47:1557–1589
- Bryan S, Martí J, Cas R (1998) Stratigraphy of the Bandas del Sur Formation: an extracaldera record of quaternary phonolitic explosive eruptions from the Las Cañadas edifice, Tenerife (Canary Islands). *Geol Mag* 135:605–636
- Bryan S, Martí J, Leosson M (2002) Petrology and geochemistry of the bandas del Sur formation, Las Cañadas edifice, Tenerife (Canary Islands). *J Petrol* 43:1815–1856
- Carracedo JC, Badiola ER, Guillou H, Paterne M, Scaillet S, Torrado FP, Paris R, Fra-Paleo U, Hansen A (2007) Eruptive and structural history of the Aede Volcano and rift zones of Tenerife, Canary Islands. *Geol Soc Am Bull* 119:1027–1051
- Dávila-Harris P (2009) Explosive ocean-island volcanism: the 1.8–0.7 Ma explosive eruption history of Cañadas volcano recorded by the pyroclastic successions around Adeje and Abona, southern Tenerife, Canary Islands. University of Leicester
- Dávila-Harris P, Ellis BS, Branney MJ, Carrasco-Núñez G (2013) Lithostratigraphic analysis and geochemistry of a vitric spatter-bearing ignimbrite: the Quaternary Adeje Formation, Cañadas volcano, Tenerife. *Bull Volcanol* 75:1–15
- De Silva S, Francis P (1989) Correlation of large ignimbrites—two case studies from the Central Andes of Northern Chile. *J Volcanol Geotherm Res* 37:133–149
- Desborough GA, Pitman JK, Donnell JR (1973) Microprobe analysis of biotites—A method of correlating tuff beds in the Green River Formation, Colorado and Utah. *Journal of Research of the US Geological Survey* 1(1):39–44
- Donato P, Albert P, Crocitti M, De Rosa R, Menzies M (2016) Tephra layers along the southern Tyrrhenian coast of Italy: links to the X-5 & X-6 using volcanic glass geochemistry. *J Volcanol Geotherm Res* 317:30–41
- Dorais MJ, Whitney JA, Stormer JC Jr (1991) Mineralogical constraints on the petrogenesis of trachytic inclusions, Carpenter ridge tuff, Central San Juan volcanic field, Colorado. *Contrib Mineral Petrol* 107:219–230
- Dymek R (1983) Titanium, aluminum and interlayer cation substitutions in biotite from high-grade gneisses' West Greenland. *Am Mineral* 68:880–899
- Edgar CJ, Wolff JA, Nichols H, Cas R, Martí J (2002) A complex quaternary ignimbrite-forming phonolitic eruption: the Poris member of the Diego Hernández Formation (Tenerife, Canary Islands). *J Volcanol Geotherm Res* 118:99–130

- Edgar CJ, Wolff JA, Olin PH, Nichols H, Pittari A, Cas R, Reiners P, Spell T, Marti J (2007) The late Quaternary Diego Hernandez Formation, Tenerife: volcanology of a complex cycle of voluminous explosive phonolitic eruptions. *J Volcanol Geotherm Res* 160:59–85
- Eichelberger JC, Chertkoff DG, Dreher ST, Nye CJ (2000) Magmas in collision: rethinking chemical zonation in silicic magmas. *Geology* 28:603–606
- Ellis BS, Mark DF, Pritchard CJ, Wolff JA (2012) Temporal dissection of the Huckleberry Ridge Tuff using the 40 Ar/39 Ar dating technique. *Quat Geochronol* 9:34–41
- Ewart A, Griffin W (1994) Application of proton-microprobe data to trace-element partitioning in volcanic rocks. *Chem Geol* 117:251–284
- Forni F, Bachmann O, Mollo S, De Astis G, Gelman SE, Ellis BS (2016) The origin of a zoned ignimbrite: insights into the Campanian Ignimbrite magma chamber (Campi Flegrei, Italy). *Earth Planet Sci Lett* 449:259–271
- Forni F, Ellis BS, Bachmann O, Lucchi F, Tranne CA, Agostini S, Dallai L (2015) Erupted cumulate fragments in rhyolites from Lipari (Aeolian Islands). *Contrib Mineral Petrol* 170:1–18
- Francalanci L, Taylor S, McCulloch M, Woodhead J (1993) Geochemical and isotopic variations in the calc-alkaline rocks of Aeolian arc, southern Tyrrhenian Sea, Italy: constraints on magma genesis. *Contrib Mineral Petrol* 113:300–313
- Guillong M, Meier D, Allan M, Heinrich C, Yardley B (2008) SILLS: a MATLAB-based program for the reduction of laser ablation ICP-MS data of homogeneous materials and inclusions. *Mineralogical Association of Canada Short Course* 40:328–333
- Harangi S, Mason PR, Lukács R (2005) Correlation and petrogenesis of silicic pyroclastic rocks in the Northern Pannonian Basin, Eastern-Central Europe: in situ trace element data of glass shards and mineral chemical constraints. *J Volcanol Geotherm Res* 143:237–257
- Haynes JT, Melson WG, Kunk MJ (1995) Composition of biotite phenocrysts in Ordovician tephra casts doubt on the proposed trans-Atlantic correlation of the Millbrig K-bentonite (United States) and the Kinnekulle K-bentonite (Sweden). *Geology* 23(9):847
- Hazen R, Wones D (1972) Effect of cation substitutions on physical properties of trioctahedral micas. *Am Mineral* 57:103–129
- Hildreth W (1979) The Bishop Tuff: evidence for the origin of compositional zonation in silicic magma chambers. *Geol Soc Am Spec Pap* 180:43–75
- Hildreth W (1981) Gradients in silicic magma chambers: implications for lithospheric magmatism. *J Geophys Res: Solid Earth* 86:10153–10192
- Hildreth W, Moorbath S (1988) Crustal contributions to arc magmatism in the Andes of central Chile. *Contrib Mineral Petrol* 98:455–489
- Hoernle K (1998) Geochemistry of Jurassic oceanic crust beneath Gran Canaria (Canary Islands): implications for crustal recycling and assimilation. *J Petrol* 39:859–880
- Hunt J, Talling P, Clare M, Jarvis I, Wynn R (2014) Long-term (17 Ma) turbidite record of the timing and frequency of large flank collapses of the Canary Islands. *Geochem Geophys Geosyst* 15:3322–3345
- Huertas MJ, Arnaud NO, Ancochea E, Cantagrel JM, Fuster JM (2002) <sup>40</sup>Ar/<sup>39</sup>Ar stratigraphy of pyroclastic units from the Cañadas Volcanic Edifice (Tenerife, Canary Islands) and their bearing on the structural evolution. *J Volcanol Geotherm Res* 115(3):351–365
- Le Friant A, Ishizuka O, Boudon G, Palmer M, Talling P, Villemant B, Adachi T, Aljahdali M, Breitkreuz C, Brunet M (2015) Submarine record of volcanic island construction and collapse in the lesser Antilles arc: first scientific drilling of submarine volcanic island landslides by IODP Expedition 340. *Geochem Geophys Geosyst* 16:420–442
- Lipman PW (1967) Mineral and chemical variations within an ash-flow sheet from Aso caldera, southwestern Japan. *Contrib Mineral Petrol* 16:300–327
- Luhr JF, Carmichael IS (1980) The colima volcanic complex, Mexico. *Contrib Mineral Petrol* 71:343–372
- Mahood GA, Hildreth W (1986) Geology of the peralkaline volcano at Pantelleria, Strait of Sicily. *Bull Volcanol* 48:143–172
- Mark DF, Petraglia M, Smith VC, Morgan LE, Barfod DN, Ellis BS, Pearce NJ, Pal J, Korisettar R (2014) A high-precision 40 Ar/39 Ar age for the young Toba tuff and dating of ultra-distal tephra: forcing of quaternary climate and implications for hominin occupation of India. *Quat Geochronol* 21:90–103
- Martí J, Mitjavila J, Araña V (1994) Stratigraphy, structure and geochronology of the las Cañadas caldera (Tenerife, Canary Islands). *Geol Mag* 131:715–727
- Martí J, Mitjavila J, Villa I (1990) Stratigraphy and K-Ar ages of the Diego Hernández wall and their significance on the Las Cañadas Caldera formation (Tenerife, Canary Islands). *Terra Nov.* 2:148–153
- Mason BG, Pyle DM, Oppenheimer C (2004) The size and frequency of the largest explosive eruptions on Earth. *Bull Volcanol* 66:735–748
- McIntosh WC, Sutter JF, Chapin CE, Kedzie LL (1990) High-precision 40Ar/39Ar sanidine geochronology of ignimbrites in the Mogollon-Datil volcanic field, southwestern New Mexico. *Bull Volcanol* 52:584–601
- Menard HW (1956) Archipelagic aprons. *AAPG Bull* 40:2195–2210
- Mitjavila J (1990) Aplicació de tècniques de geoquímica isotòpica i de geocronologia a l'estudi volcànic de l'edifici de Diego Hernández i la seva relació amb la Caldera de Las Cañadas (Tenerife). PhD thesis, Univ. of Barcelona (microfilm no. 1312), Spain
- Nash W, Crecraft H (1985) Partition coefficients for trace elements in silicic magmas. *Geochim Cosmochim Acta* 49:2309–2322
- Olin PH (2007) Magma dynamics of the phonolitic Diego Hernández Formation, Tenerife, Canary Islands. Washington State University
- Olin PH, Wolff JA (2012) Partitioning of rare earth and high field strength elements between titanite and phonolitic liquid. *Lithos* 128:46–54
- Ort MH, Porreca M, Geissman JW (2015) The use of palaeomagnetism and rock magnetism to understand volcanic processes: introduction. *Geol Soc Lond, Spec Publ* 396:1–11
- Pearce NJ, Westgate JA, Perkins WT (1996) Developments in the analysis of volcanic glass shards by laser ablation ICP-MS: quantitative and single internal standard-multielement methods. *Quat Int* 34:213–227
- Robertson A, Stillman C (1979) Late Mesozoic sedimentary rocks of Fuerteventura, Canary Islands: implications for West African continental margin evolution. *J Geol Soc* 136:47–60
- Sarna-Wojcicki AM, Bowman H, Meyer CE, Russell P, Woodward M, McCoy G, Rowe Jr J, Baedeker P, Asaro F, Michael H (1984) Chemical analyses, correlations, and ages of upper Pliocene and Pleistocene ash layers of east-central and southern California
- Schmincke HU, Sumita M (1998) Volcanic evolution of Gran Canaria Reconstructed from apron sediments: Synthesis of Vicap Project Drilling 27
- Schoene B, Guex J, Bartolini A, Schaltegger U, Blackburn TJ (2010) Correlating the end-Triassic mass extinction and flood basalt volcanism at the 100 ka level. *Geology* 38:387–390
- Shane P (2000) Tephrochronology: a New Zealand case study. *Earth Sci Rev* 49:223–259
- Shane P, Smith V, Naim I (2003) Biotite composition as a tool for the identification of quaternary tephra beds. *Quat Res* 59:262–270
- Sliwinski J (2014) Eruption of shallow crystal cumulates during Caldera-forming events on Tenerife, Canary Islands. ETH
- Sliwinski JT, Bachmann O, Ellis BS, Dávila-Harris P, Nelson BK, Dufek J (2015) Eruption of shallow crystal cumulates during explosive phonolitic eruptions on Tenerife, Canary Islands. *J Petrol* 56:2173–2194
- Smith VC, Isaia R, Pearce N (2011a) Tephrostratigraphy and glass compositions of post-15 kyr Campi Flegrei eruptions: implications for

- eruption history and chronostratigraphic markers. *Quat Sci Rev* 30: 3638–3660
- Smith VC, Pearce NJ, Matthews NE, Westgate JA, Petraglia MD, Haslam M, Lane CS, Korisettar R, Pal J (2011b) Geochemical fingerprinting of the widespread Toba tephra using biotite compositions. *Quat Int* 246:97–104
- Smith VC, Shane P, Smith I (2002) Tephrostratigraphy and geochemical fingerprinting of the Mangaone subgroup tephra beds, Okataina volcanic centre, New Zealand. *N Z J Geol Geophys* 45:207–219
- Solana MC (2012) Development of unconfined historic lava flow fields in Tenerife: implications for the mitigation of risk from a future eruption. *Bull Volcanol* 74:2397–2413
- Stepanov AS, Hermann J (2013) Fractionation of Nb and Ta by biotite and phengite: implications for the “missing Nb paradox”. *Geology* 41:303–306
- Szymanowski D, Ellis BS, Bachmann O, Guillong M, Phillips WM (2015) Bridging basalts and rhyolites in the Yellowstone–Snake River Plain volcanic province: the elusive intermediate step. *Earth Planet Sci Lett* 415:80–89
- Thirlwall M, Singer B, Marriner G (2000) <sup>39</sup>Ar–<sup>40</sup>Ar ages and geochemistry of the basaltic shield stage of Tenerife, Canary Islands, Spain. *J Volcanol Geotherm Res* 103:247–297
- Ukstins-Peate I, Baker JA, Kent AJ, Al-Kadasi M, Al-Subbary A, Ayalew D, Menzies M (2003) Correlation of Indian Ocean tephra to individual Oligocene silicic eruptions from Afro-Arabian flood volcanism. *Earth Planet Sci Lett* 211:311–327
- Vidal CM, Komorowski JC, Métrich N, Pratomo I, Kartadinata N, Prambada O, Michel A, Carazzo G, Lavigne F, Rodysill J (2015) Dynamics of the major plinian eruption of Samalas in 1257 AD (Lombok, Indonesia). *Bull Volcanol* 77:1–24
- Villemant B (1988) Trace element evolution in the Phlegrean Fields (Central Italy): fractional crystallization and selective enrichment. *Contrib Mineral Petrol* 98:169–183
- Walker G (1981) Plinian eruptions and their products. *Bull Volcanol* 44: 223–240
- Waters AC (1961) Stratigraphic and lithologic variations in the Columbia River basalt. *Am J Sci* 259:583–611
- Watts A, Masson D (1995) A giant landslide on the north flank of Tenerife, Canary Islands. *J Geophys Res: Solid Earth* 100:24487–24498
- Westgate J, Perkins W, Fuge R, Pearce N, Wintle A (1994) Trace-element analysis of volcanic glass shards by laser ablation inductively coupled plasma mass spectrometry: application to tephrochronological studies. *Appl Geochem* 9:323–335
- Williams R, Branney MJ, Barry TL (2014) Temporal and spatial evolution of a waxing then waning catastrophic density current revealed by chemical mapping. *Geology* 42:107–110
- Wolff JA (1985) Zonation, mixing and eruption of silica-undersaturated alkaline magma: a case study from Tenerife, Canary Islands. *Geol Mag* 122:623–640
- Wolff JA, Ellis BS, Ramos F, Starkel W, Boroughs S, Olin PH, Bachmann O (2015) Remelting of cumulates as a process for producing chemical zoning in silicic tuffs: A comparison of cool, wet and hot, dry rhyolitic magma systems. *Lithos* 275–286
- Wolff JA, Grandy J, Larson P (2000) Interaction of mantle-derived magma with island crust? Trace element and oxygen isotope data from the Diego Hernandez Formation, Las Cañadas, Tenerife. *J Volcanol Geotherm Res* 103:343–366
- Wolff JA, Storey M (1984) Zoning in highly alkaline magma bodies. *Geol Mag* 121:563–575
- Wömer G, Schmincke H (1984) Mineralogical and chemical zonation of the Laacher see tephra sequence (East Eifel, W. Germany). *J Petrol* 25:805–835
- Wotzlaw JF, Hüsing SK, Hilgen FJ, Schaltegger U (2014) High-precision zircon U–Pb geochronology of astronomically dated volcanic ash beds from the Mediterranean Miocene. *Earth Planet Sci Lett* 407: 19–34
- Yen FS, Goodwin JH (1976) Correlation of tuff layers in the Green River Formation, Utah using biotite compositions. *J Sediment Res* 46(2): 345–354